Observational Study

Medicine®

OPEN

Applicability of readout-segmented echoplanar diffusion weighted imaging for prostate MRI

Susanne Hellms, MD[a,*], Marcel Gutberlet, PhD[a], Matti Joonas Peperhove, MD[a], Stefanie Pertschy, MD[a], Christoph Henkenberens, MD[b], Inga Peters, MD[c], Frank Wacker, MD[a], Katja Derlin, MD[a]

Abstract

To evaluate readout-segmented echoplanar (rsEPI) diffusion weighted imaging (DWI) for multiparametric (mp) magnetic resonance imaging (MRI) of the prostate compared to the established single-shot echoplanar imaging (ssEPI) sequence.

One hundred ten consecutive patients with clinical suspicion of prostate cancer underwent mp prostate MRI using both, the ssEPI and the rsEPI DWI sequence. For an objective assessment, delineation of the prostate shape on both DWI sequences was compared to T2-weighted images by measuring organ diameters. Apparent diffusion coefficient (ADC) values, image contrast and contrast-to-noise ratio (CNR) were compared between the 2 sequences on a region-of-interest-based analysis. Diagnostic accuracy for quantitative ADC-values was calculated. Histopathology from MRI/ultrasound fusion-guided biopsy was used as reference standard. For a subjective assessment, 2 independent readers visually assessed image quality of both sequences using Likert-scales.

Delineation of the prostate shape was more accurate with rsEPI compared to ssEPI. ADC values in target lesions were not significantly different but significantly higher in the surrounding normal prostatic tissue of the transition zone. CNR was comparable between ssEPI and rsEPI. Sensitivity and specificity were good for both sequences with 84/84% and 82/73% with a Youden selected cut-off of ADC = $0.971*10^{-3}$ mm^2/s for rsEPI and $1.017*10^{-3}$ mm^2/s for ssEPI. Anatomic artifacts were significantly less and SNR was lower on rsEPI compared to ssEPI in the subjective analysis.

Delineation of the prostate shape was more accurate with rsEPI DWI than with ssEPI DWI with less anatomic artifacts and higher subjective SNR and image quality on rsEPI DW images. Diagnostic ability of quantitative ADC-values was not significantly different between the 2 sequences. Thus, rsEPI DWI might be more suitable for prostate MRI with regard to MRI-guided targeted biopsy and therapy planning.

Abbreviations: ACR = American College of Radiology, ADC = apparent diffusion coefficient, ANOVA = analysis of variance, AUC = area under the curve, CNR = contrast to noise ratio, cov = coefficient of variance, DCE = dynamic contrast enhancement, DWI = diffusion weighted imaging, ESUR = European Society of Urogenital Radiology, ICC = intraclass correlation coefficient, MRI = magnetic resonance imaging, ns = not significant, PCa = prostate carcinoma, PI-RADS = prostate imaging and reporting archiving data system, PSA = prostate specific antigen, pz = peripheral zone, ROI = region of interest, rsEPI = readout-segmented echoplanar imaging, SD = standard deviation, SNR = signal to noise ratio, ssEPI = single-shot echoplanar imaging, TSE = turbo spin echo, tz = transitional zone.

Keywords: diffusion weighted imaging, MRI/ultrasound fusion-guided biopsy, prostate MRI, readout-segmented echoplanar imaging

1. Introduction

Over the last 10 years, rising expertise in multiparametric (mp) magnetic resonance imaging (MRI) for diagnostics of prostate cancer (PCa) has been gained. High accuracy for the detection of PCa could be achieved[1–4] due to advances in software and hardware of MRI machines, ongoing optimization of MRI protocols, as well as standardization of acquisition, interpretation, and reporting of mpMRI.[5] mpMRI including T2-weighted imaging, diffusion weighted imaging (DWI) and dynamic contrast-enhanced imaging (DCE) achieves tumor detection rates of 80% to 100% for PCa with a Gleason score >7, 63% to 97% for a Gleason score of 7 and 21% to 75% for a Gleason score of 6.[6] DWI provides highest accuracy for the detection of PCa if only 1 sequence is considered[7–11] and correlates with the cellularity of PCa.[11] Furthermore, targeted MRI/ultrasound fusion-biopsy has been reported to improve the detection of significant PCa,[3,12,13] but the anatomical correct shape of the prostate on MR images is required in order to assure accurate image fusion and enable precise lesion targeting.

For abdominal DWI in a clinical setting, the standard single-shot (ss) echoplanar imaging (EPI) pulse sequence is usually applied, even though it is known to be sensitive to susceptibility

Editor: Neeraj Lalwani.

Frank Wacker, Marcel Gutberlet, and Katja Derlin have research collaborations with Siemens healthcare outside the submitted work.

Susanne Hellms and Katja Derlin received funding from the Young faculty program of Hannover Medical School.

The authors have no conflicts of interest to disclose.

Supplemental Digital Content is available for this article.

[a] Institute for Diagnostic and Interventional Radiology, [b] Institute for Radiation Therapy and Special Oncology, [c] Clinic for Urology and urologic Oncology, Hannover Medical School, Hannover, Germany.

[*] Correspondence: Susanne Hellms, Institute for Diagnostic and Interventional Radiology, Hannover Medical School, Carl-Neuberg Str. 1, 30625 Hannover, Germany (e-mail: Hellms.Susanne@mh-hannover.de).

Copyright © 2019 the Author(s). Published by Wolters Kluwer Health, Inc. This is an open access article distributed under the terms of the Creative Commons Attribution-Non Commercial-No Derivatives License 4.0 (CCBY-NC-ND), where it is permissible to download and share the work provided it is properly cited. The work cannot be changed in any way or used commercially without permission from the journal.

Medicine (2019) 98:29(e16447)

Received: 6 March 2019 / Received in final form: 19 June 2019 / Accepted: 20 June 2019

http://dx.doi.org/10.1097/MD.0000000000016447

artifacts at tissue interfaces and increased blurring, particularly at higher field strengths. Inhomogeneity of the magnetic field may arise at tissue interfaces within materials with unequal properties (prostate tissue vs air-filled rectum vs metal implants; eg, hip prosthesis), resulting in inhomogeneous precipitation of spins and increased free induction decay.[14]

For prostate MRI, the advantages of 3T with increased spatial and temporal resolution are preferred,[5] even though artifacts might be fewer at lower magnetic field strengths.[14] In cases of prostate MRI, in which the suspicious lesion is only visible on DWI, distortion and susceptibility artifacts can lead to challenging tasks when it comes to biopsy planning. Therefore, the implementation of alternative techniques to acquire DWI sequences, which are less susceptible to artifacts but have comparable image quality, are desirable. A promising diffusion technique is the readout-segmented (rs) EPI DWI sequence showing high image quality and reduced image artifacts[14] in breast MRI examinations[15] and in several head-and-neck studies,[16–19] but so far, in only few subjective evaluations of prostate MRI in healthy volunteers[20] or in a clinical setting.[21]

The purpose of our study was the prospective, objective, and subjective evaluation of the rsEPI DWI sequence in comparison to the standard ssEPI DWI sequence for prostate MRI.

2. Material and methods

2.1. Subjects

This prospective study was approved by the local ethics committee of Hannover Medical School (7276-2017) and written informed consent was obtained from each patient. One hundred ten consecutive patients with clinical suspicion of PCa due to positive screening test (prostate-specific antigen [PSA] elevation, suspicious digital rectal examination) or under active surveillance underwent prostate MRI. In case of suspicious lesions, visible on MRI, targeted MRI/ultrasound fusion-guided biopsy was performed using the BioJet™ fusion system and software (D&K Technologies, Barum, Germany) containing 1 to 3 biopsy cores per lesion as well as additional random biopsy cores as described previously.[22–24]

2.2. Imaging protocol

All MRI examinations were performed on a 3T MRI machine (MAGNETOM Skyra, Siemens Healthcare, Erlangen, Germany). Each patient received a complete mpMRI of the prostate, according to recommendations of the American College of Radiology (ACR), the AdMeTech Foundation and the European Society of Urogenital Radiology (ESUR),[5] including T2 turbo spin echo (TSE) images in 3 planes, DWI, dynamic contrast-enhanced images, each with a slice thickness of 3 mm as well as T1 weighted spoiled gradient echo images before and after contrast medium administration. For this study, 2 different DWI sequences were conducted in each patient, using the standard ssEPI technique and the rsEPI technique. For both, the Stejskal–Tanner pulsed gradient spin echo[25] technique was used to sensitize the sequence for diffusion. The phase encoding direction was anterior–posterior for both diffusion techniques.

To reduce distortion- and motion-induced phase errors, the rsEPI technique comprised a 2-dimensional navigator echo included in a second spin-echo (the echo-train used for imaging was placed in the first spin-echo of the dual spin-echo). The 2D-navigator based reacquisition process initiates the repetition of scans that result in unusable data by using the width of the signal distribution in the readout direction as a metric for the extent of the nonlinear phase error in real-time.[14] Furthermore, for the rsEPI sequence, the k-space trajectory is divided into multiple segments (n = 5) in the readout direction, leading to shorter TE times corresponding to the reduced k-space coverage per shot. Still, rsEPI DWI results in longer total acquisition times compared to the ssEPI, which performs the k-space trajectory in a ss technique. In order to make expenditure of time for DWI with both techniques comparable, we used 2 *b*-values (0, 1000 s/mm^2) for the rsEPI, resulting in an acquisition time of 7 minutes and 47 seconds and 3 *b*-values (0, 400, 1000 s/mm^2) for the ssEPI, resulting in an acquisition time of 6 minutes and 32 seconds. Detailed parameters for both DWI sequences are given in Table 1.

ADC maps were calculated according to the mono-exponential fit, using the integrated Siemens software. ADC maps for rsEPI were calculated from 2 *b*-values (0, 1000 s/mm^2). For the ssEPI, 2 sets of ADC maps were calculated: first, using 3 *b*-values (0, 400, 1000 s/mm^2), second, in order to exclude bias that could result from the different number of *b*-values for the 2 sequences, additional ADC maps with 2 *b*-values (0, 1000 s/mm^2) were calculated.

2.3. Objective evaluation of image properties of diffusion sequences

2.3.1. Anatomic shape. Delineation of prostate contours on transversal T2 TSE images was defined as gold standard for the

Table 1

Sequence parameters for single-shot and readout-segmented echo-planar DWI.

Sequence parameter	ssEPI DWI	rsEPI DWI
TR/TE, ms	6300/76	6380/64
Slice thickness, mm	3	3
Number of averages (NEX)	3 (b = 0 s/mm^2), 6 (b = 400 s/mm^2), 12 (b = 1000 s/mm^2)	1 (b = 0 s/mm^2), 3 (b = 1000 s/mm^2)
FOV, mm	220 × 220	220 × 220
Flip angle, °	90	90
b-values, s/mm^2	0, 400, 1000	0, 1000
Number of readout segments	1	5
Acquisition time, min.s	6.32	7.47
Fat suppression	SPAIR	SPAIR
Parallel imaging	GRAPPA: acceleration Factor = 2	GRAPPA: acceleration Factor = 2
Bandwidth, Hz/pixel	1190	850
Phase encoding direction	Anterior–posterior	Anterior–posterior

FOV = field of view, rsEPI = readout-segmented echo-planar imaging, ssEPI = single-shot echo-planar imaging, SPAIR = spectral attenuated inversion recovery, TE = echo time, TR = repetition time.

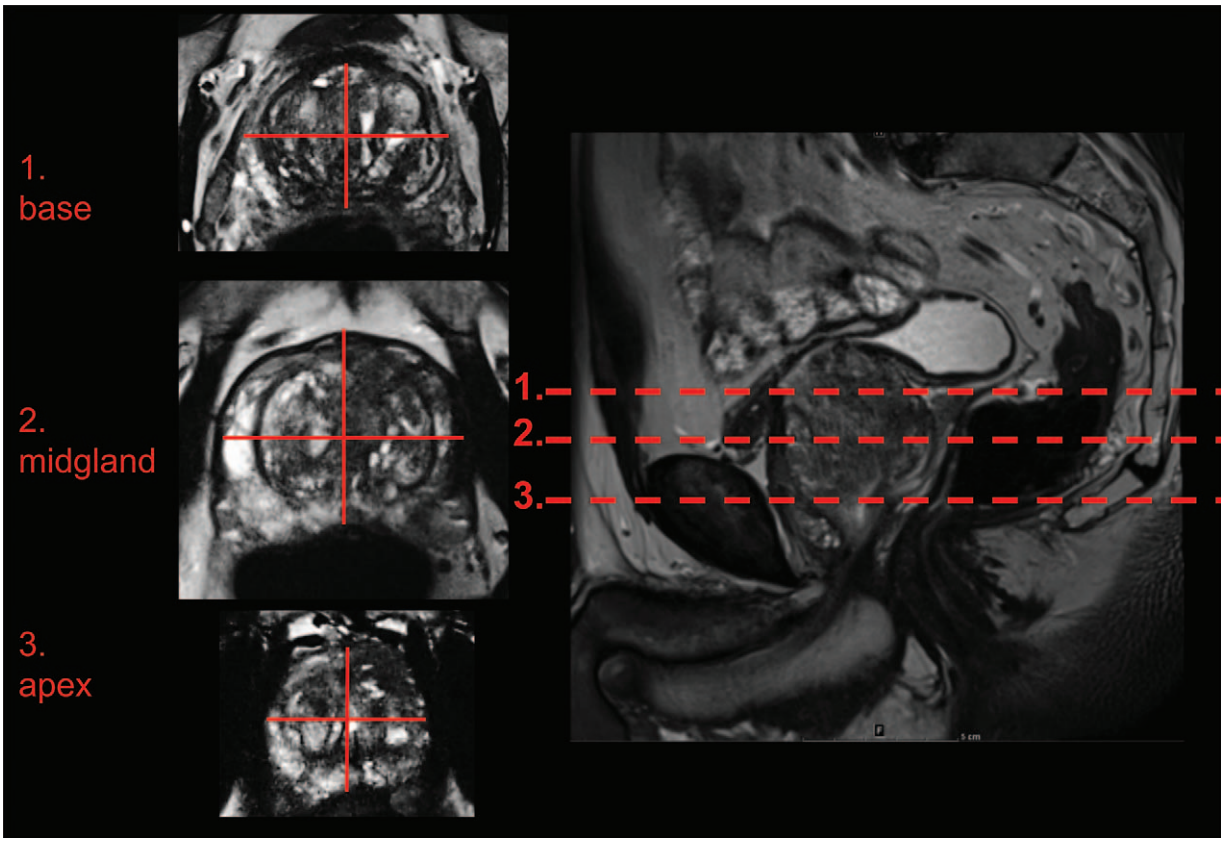

Figure 1. Measurement of prostate diameters was performed in 3 planes. Measurement of prostate diameters was performed in the prostate base, midgland, and prostate apex in anterior–posterior and right–left orientation as depicted.

correct anatomic shape of the prostate. To compare delineation of the prostate on T2-images with ssEPI and rsEPI, diameters were drawn manually in right–left and anterior–posterior orientation in 3 planes: the prostate base, midgland, and apex on each sequence (Fig. 1).

2.3.2. Signal intensity. Regions-of-interest (ROIs) were placed manually in the suspicious lesion as well as in the normal tissue of the peripheral zone (pz) and the transition zone (tz) on b1000 images and ADC maps of both, the ssEPI and the rsEPI.

2.3.3. Contrast and contrast-to-noise ratio. Contrast of diffusion images was determined from the above-mentioned signal intensity measurements where signal (lesion) is the ROI-based determined signal in a suspicious lesion and signal (tissue) is the signal of the adjacent normal prostatic tissue of the particular anatomic zone of the prostate where the suspicious lesion is located. The following equation was used to calculate image contrast:

$$\text{contrast} = \text{signal(lesion)}/\text{signal(tissue)},$$

Contrast-to-noise ratio (CNR) was also calculated from the above-mentioned signal intensity measurements where SD (lesion) is the ROI-based determined standard deviation in a suspicious lesion and SD (tissue) is the standard deviation in the adjacent normal prostatic tissue of the particular anatomic zone of the prostate where the suspicious lesion is located.

The following equation was used to determine CNR[26]:

$$\text{CNR} = \frac{\text{signal(tissue)} - \text{signal(lesion)}}{\sqrt{\text{SD(tissue)}^2 + \text{SD(lesion)}^2}},$$

2.4. Subjective evaluation of image properties of diffusion sequences parameters

MR-studies with clinical suspicion of PCa were analyzed by 2 readers, experienced in prostate MRI, in 2 sessions. Both readers were blinded to clinical data and biopsy results. In the first session, MRI data sets were analyzed using either ssEPI or rsEPI in an alternating, predefined order using standardized hanging protocols. At least 1 week after the first reading session, the second session was performed using the other DWI sequence, again in an alternating, predefined order. The following characteristics were assessed using a 5-point Likert-scale (1 = nondiagnostic, 2 = poor, 3 = satisfactory, 4 = good, 5 = excellent): degree of ghosting and susceptibility, subjective signal-to-noise ratio (SNR), subjective anatomic distortion (distortion in size, profile or orientation), image sharpness (defined as clear depiction of prostate edge), differentiation of pz and tz and overall image quality. Furthermore, diagnostic certainty to distinguish PCa from benign prostatic tissue was evaluated using the same Likert-scale for ssEPI and rsEPI under consideration of T2-weighted images and DCE since the

probability of PCa is usually assessed with mpMRI in a clinical setting.

2.5. Statistical analysis

Statistical analysis was performed using SPSS software version 24 (IBM, NY), Prism software version 5 (GraphPad, CA) and MedCalc software version 17.9.7 (MedCalc, Ostend, Belgium). Normal distribution of data was tested according to Kolmogorov–Smirnov tests and parametric (analysis of variance [ANOVA], *t* test) or nonparametric tests (Friedman test, Wilcoxon rank sum test) were chosen accordingly. For the evaluation of the agreement of prostate diameters between T2-weighted images and ssEPI as well as T2-weighted images and rsEPI, the coefficient of variation (cov) and the intraclass correlation coefficient (ICC) was calculated for each diameter. For the comparison of ADC values, image contrast and CNR measured on ssEPI and rsEPI, paired *t* tests, Wilcoxon rank sum tests, repeated measures ANOVA (with Bonferroni-correction) or Friedman tests were performed. Receiver operating characteristic curves were generated to evaluate diagnostic ability of ADC values from ssEPI and rsEPI DW images in differentiating benign prostate tissue from PCA, and area under curves (AUC) was compared using the method of DeLong et al.[27] Parameters from qualitative evaluations were compared using Wilcoxon rank sum tests. *P*-values $<.05$ were considered statistically significant. Values are given as mean ± standard error of the mean, if not indicated differently.

3. Results

3.1. Clinical parameters

MRI examinations of 110 men (mean ± standard deviation: age: 69 ± 9 years, PSA 8.7 ± 5.6 ng/ml) were included in the study. In 53/110 MRI scans, suspicious or indeterminate lesions (prostate imaging and reporting archiving data system [PI-RADS] ≥3) were described in the initial clinical assessment (n = 14 with PI-RADS 3 and n = 39 with PI-RADS 4 or 5). In 42/53 of patients with PI-RADS ≥3, histopathological results were available from MRI/ultrasound fusion-guided biopsy. 31/42 patients were diagnosed with PCa (n = 8 with Gleason 3 + 3 = 6, n = 23 with Gleason ≥3 + 4 = 7). In 11/53 patients, histopathology from MRI/ultrasound fusion-guided biopsy was not available; these patients underwent untargeted biopsy or were biopsied outside of our institution, underwent transurethral laser excision of the prostate or were lost to follow-up.

3.2. Prostate diameters on rsEPI agreed significantly better than on ssEPI DW images with diameters on T2-weighted images

Depending on the plane and orientation of the measurement, COV between diameters on T2-weighted and rsEPI DW images were lower (range 3%–6%) than COV between diameters on T2-weighted images and ssEPI DW images (range 4%–9%). Differences were particularly evident in anterior–posterior diameters (rsEPI DWI: range 4%–5% vs ssEPI DWI: range 8%–9%) compared to right–left diameters (rsEPI DWI: range 3%–6% vs ssEPI DWI: range 4%–5%).

The ICC between T2 and rsEPI DWI was higher (range 0.96–0.98) than ICC between T2 and ssEPI DWI (range 0.90–0.97, Table 2) and differences were more distinct in anterior–posterior diameters (rsEPI DWI: range 0.96–0.98 vs ssEPI DWI: range 0.90–0.92) compared to right–left diameters (rsEPI DWI: range 0.96–0.98 vs ssEPI DWI: range 0.96–0.97). Visual comparison of rsEPI DWI and ssEPI DWI in 3 MRI examinations is depicted in Figure 2.

3.3. ADC values in target lesions were not significantly different while ADC values of the tz were higher on rsEPI compared to ssEPI

No difference was found in the comparison of ADC values of ssEPI ADC maps with 2 ($b = 0$, 1000 s/mm^2) or 3 ($b = 0$, 400, 1000 s/mm^2) *b*-values in the pz, the tz or in the target lesion. Therefore, we focused on results of only 1 set of ssEPI ADC maps ($b = 0$, 400, 1000 s/mm^2). Results of all calculated ADC maps are given in Supplement Table 1, http://links.lww.com/MD/D117. ADC values in the normal tissue of the tz were significantly higher on rsEPI ($1.43 \pm 0.02 * 10^{-3}$ mm^2/s) compared to ssEPI ($1.32 \pm 0.03 * 10^{-3}$ mm^2/s, $P < .001$). ADC values in the pz on rsEPI ($1.85 \pm 0.04 * 10^{-3}$ mm^2/s) were not significantly different compared to ssEPI ($1.82 \pm 0.03 * 10^{-3}$ mm^2/s, not significant (ns), $P = .3$). ADC values measured in the suspicious lesions did not show significant differences between rsEPI ($0.90 \pm 0.04 * 10^{-3}$ mm^2/s) and ssEPI ($0.94 \pm 0.06 * 10^{-3}$ mm^2/s, ns, $P = .2$, Table 3).

3.4. Image contrast was significantly higher on b1000 images of rsEPI compared to ssEPI

Calculation of image contrast resulted in significantly higher values in b1000 images of rsEPI compared to ssEPI (1.47 ± 0.05 vs 1.23 ± 0.04, $P < .001$). No significant difference in image

Table 2

Variability of organ diameters measured on ssEPI DWI and rsEPI DWI sequences.

		cov		ICC	
Plane	**Organ diameter**	**ssEPI DWI**	**rsEPI DWI**	**ssEPI DWI**	**rsEPI DWI**
Base	Right–left	0.04 ± 0.004	0.03 ± 0.003**	0.97	0.98
	Anterior–posterior	0.08 ± 0.007	0.04 ± 0.004***	0.90	0.96
Midgland	Right–left	0.04 ± 0.004	0.03 ± 0.095***	0.96	0.96
	Anterior–posterior	0.08 ± 0.008	0.04 ± 0.004***	0.91	0.96
Apex	Right–left	0.07 ± 0.007	0.06 ± 0.006***	0.96	0.98
	Anterior–posterior	0.09 ± 0.009	0.05 ± 0.005***	0.92	0.98

Presented are coefficients of variation and intraclass correlation coefficients for measurements of organ diameters of all conducted MRI studies (n = 110). Prostate diameters from T2 images were compared to diameters from ssEPI and rsEPI DW images. Comparison of COV was performed using paired *t* tests.

cov = coefficient of variation, ICC = intraclass correlation coefficient, ssEPI = single-shot echoplanar imaging, rsEPI = readout-segmented echoplanar imaging.

** $P < .01$.

*** $P < .001$.

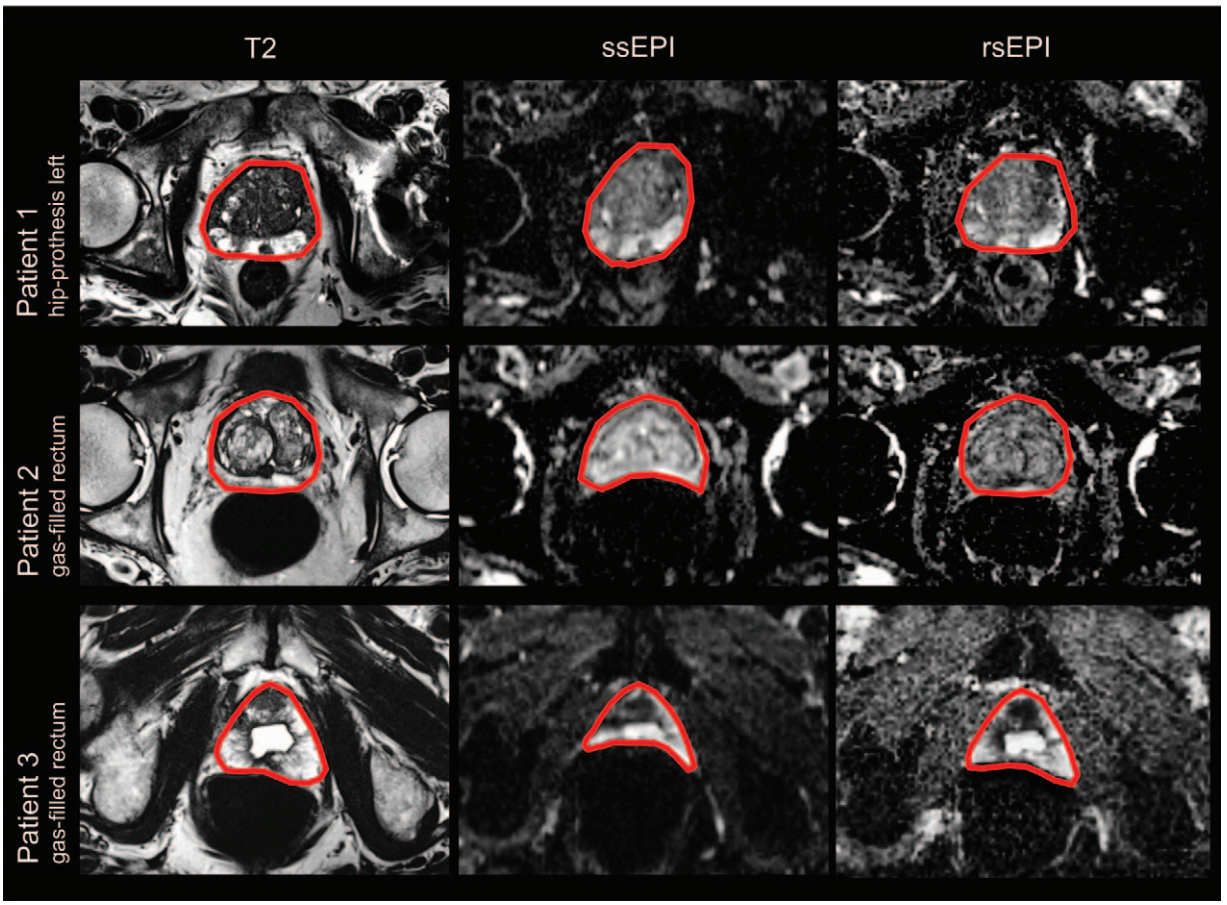

Figure 2. Visual comparison of rsEPI DWI and ssEPI DWI by means of MRI examinations from our collective. Depicted are 3 representative MRI examinations with challenging conditions for DWI. The prostate shape is delineated in red and agreement with T2 weighted images is better with rsEPI DWI than with ssEPI DWI. DWI = diffusion weighted imaging, MRI = magnetic resonance imaging, rsEPI = readout-segmented echoplanar, ssEPI = single-shot echoplanar imaging.

contrast of ADC maps was found for both calculation methods (Table 4).

A subgroup analysis of lesions located in the pz and tz revealed higher values for image contrast on rsEPI than on ssEPI images in both subgroups (Supplement Table 2, http://links.lww.com/MD/D117).

3.5. CNR was comparable on rsEPI and ssEPI DWI sequences

In the comparison of ROI-based determined signal intensities with standard deviations on ADC maps and b1000 images, calculated CNR was not significantly different on rsEPI (6.56 ± 1.28) and ssEPI (4.42 ± 0.5, ns, $P = .5$). Furthermore, CNR was not significantly different on b1000 images (Table 4).

A subgroup analysis of lesions located in the pz and tz revealed no significant difference of CNR for rsEPI and ssEPI. Results of this subgroup analysis are presented in Supplement Table 2, http://links.lww.com/MD/D117.

3.6. High diagnostic accuracy for the detection of PCA could be achieved with ADC quantification in both sequences

Sensitivities and specificities for PCA detection with ROI-based ADC measurements for rsEPI/ssEPI were 84/84% and 82/73%

Table 3

Comparison of mean ADC values in MR-studies with defined target lesions (n = 53).

	ROI	ssEPI DWI $b = 0, 400, 1000\ s/mm^2$	rsEPI DWI $b = 0, 1000\ s/mm^2$	*P*-value
ADC (10^{-3} mm^2/s)	target lesion	0.936 ± 0.055	0.900 ± 0.039	ns, .2*
	peripheral zone	1.822 ± 0.033	1.846 ± 0.036	ns, .3†
	transition zone	1.316 ± 0.029	1.425 ± 0.022	<.001†

Values are given as mean ± standard error of the mean. For ssEPI DWI ADC maps were calculated from $b = 0, 400, 1000\ s/mm^2$ values; for rsEPI DWI, ADC maps were calculated from $b = 0, 1000\ s/mm^2$ values.
ADC = apparent diffusion coefficient, rsEPI = readout-segmented echoplanar imaging, ROI = region of interest, ssEPI = single-shot echoplanar imaging.
P-values were derived from
* Wilcoxon rank sum test in case of non-Gaussian distribution of data or
† Paired *t* tests for normally distributed data.

Table 4

Comparison of image contrast and contrast-to-noise ratio in MR-examinations with defined target lesions (n = 53).

Parameter	Image sequence	ssEPI DWI	rsEPI DWI	*P*-value
Image contrast	ADC	0.55 ± 0.02	0.53 ± 0.02	ns, 1.0*
	b1000 images	1.23 ± 0.04	1.47 ± 0.05	<.001†
contrast-to-noise ratio	ADC	4.42 ± 0.50	6.56 ± 1.28	ns, .5†
	b1000 images	1.85 ± 0.03	2.24 ± 0.24	ns, .1*

Values are given as mean ± standard error of the mean. For ssEPI DWI ADC maps were calculated from $b = 0, 400, 1000$ s/mm^2 values; for rsEPI DWI, ADC maps were calculated from $b = 0, 1000$ s/mm^2 values.
ADC = apparent diffusion coefficient, rsEPI = readout-segmented echoplanar imaging, ssEPI = single-shot echoplanar imaging.
P-values were derived from
* Paired *t* tests for normally distributed data or
† Wilcoxon rank sum test in case of non-Gaussian distribution of data.

with a Youden selected cut-off value of $0.971*10^{-3}$ mm^2/s for rsEPI and $1.017*10^{-3}$ mm^2/s for ssEPI. AUC calculations revealed an area of 0.8343 (95% confidence interval 0.688–0.931) for rsEPI and 0.768 (95% confidence interval 0.613–0.884) for ssEPI (Fig. 3). The AUCs for ssEPI and rsEPI were not significantly different ($P = .55$).

3.7. rsEPI DW images had less anatomic artifacts and lower SNR compared to ssEPI DW images in the subjective analysis

The overall image quality was significantly better with rsEPI than with ssEPI (reader 1: 3.9 ± 0.1 vs 3.5 ± 0.1, $P < .05$, reader 2: 3.1 ± 0.1 vs 2.8 ± 0.2, $P < .05$, Table 5) and the degree of ghosting and susceptibility (reader 1: 4.4 ± 0.1 vs 3.7 ± 0.2, $P < .001$, reader 2: 3.2 ± 0.1 vs 2.5 ± 0.2, $P < .001$) and anatomic distortion (reader 1: 4.3 ± 0.1 vs 3.1 ± 0.2, $P < .001$, reader 2: 3.6 ± 0.1 vs 3.0 ± 0.2, $P < .01$) was significantly less in the subjective assessment of image quality as evaluated by both readers. SNR was significantly better with ssEPI than rsEPI for both readers (reader 1: 4.2 ± 0.1 vs 3.7 ± 0.1, $P < .01$, reader 2: 2.7 ± 0.1 vs 2.5 ± 0.1, $P < .05$). No significant difference was found for the image sharpness for both readers (reader 1: 3.4 ± 0.1 vs 3.5 ± 0.1, ns, $P = .4$, reader 2: 3.4 ± 0.1 vs 3.3 ± 0.1, ns, $P = .4$) and for the differentiation of the peripheral and tz for reader 2 (3.3 ± 0.1 vs 3.4 ± 0.1, ns, $P = 1.0$), while for reader 1 the differentiation of peripheral and tz was better with ssEPI DWI (4.1 ± 0.1 vs 3.7 ± 0.1, $P < .001$). Diagnostic certainty was equal with both DWI sequences for reader 1 (3.8 ± 0.1 vs 4.1 ± 0.2, ns, $P = .6$) and significantly better with rsEPI for reader 2 (3.4 ± 0.2 vs 4.0 ± 0.1, $P < .01$).

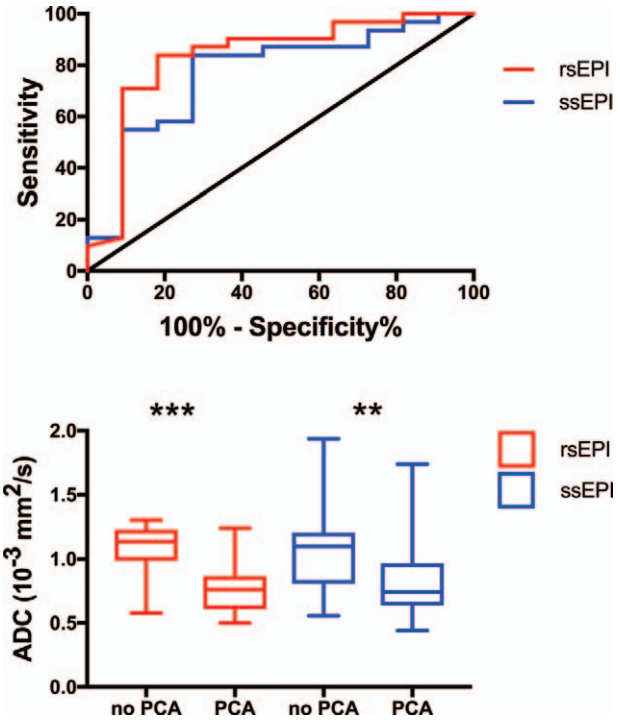

Figure 3. Comparison of areas under the curve for the detection of PCa with rsEPI DWI and ssEPI DWI and differences of ADC values in PCa positive and PCa negative target lesions for both sequences. Areas under the curve for the detection of PCa were comparable with rsEPI DWI and ssEPI DWI ($P = .55$) and ADC values were significantly lower in PCa positive lesions compared to non-PCa lesions for both sequences, $^{**}P < .01$, $^{***}P < .001$. ADC = apparent diffusion coefficient, DWI = diffusion weighted imaging, MRI = magnetic resonance imaging, PCa = prostate cancer, rsEPI = readout-segmented echo-planar, ssEPI = single-shot echoplanar imaging.

4. Discussion

We showed that delineation of the prostate shape using rsEPI DWI agreed better with the actual anatomic shape than ssEPI DWI with less anatomic artifacts and higher subjective SNR on rsEPI DW images. Both readers rated the image quality of rsEPI DWI better than of ssEPI DWI images. No significant difference between the 2 sequences was found in the objective assessment of image contrast and CNR as well as in the diagnostic ability of quantitative ADC values.

DWI is the most important MR-sequence for the diagnosis of significant PCa in the PI-RADS scoring system, being the leading sequence for the pz and the second sequence for the transitional zone.[5,28] Previous research has shown that DWI-PI-RADS scores provide highest accuracy for the detection of PCa, if only 1 sequence is considered.[7,9,29] MRI/ultrasound fusion-guided biopsy has been reported to improve detection of significant PCa compared to the untargeted ultrasound-guided biopsy method,[3,12,30,31] but the correct anatomical delineation of the prostate shape and lesion localization is essential to assure accurate image-fusion and successful biopsy.[12] Especially in cases where the target lesion is only visible on DWI, the anatomically correct shape on this sequence is required for biopsy planning and rsEPI DWI might be superior to the standard ssEPI DWI sequence. In our study, we could show that with rsEPI DWI, delineation of the prostate shape was more accurate than with ssEPI DWI, showing less anatomic artifacts and higher subjective SNR. Therefore, rsEPI DWI might be an appropriate sequence for prostate imaging. Furthermore, in order to close the gap between

Table 5

Qualitative assessment of rsEPI DWI and ssEPI DWI sequences.

Parameter	Reader	ssEPI DWI	rsEPI DWI	*P*-value
Ghosting and susceptibility	Reader 1	3.7 ± 0.2	4.4 ± 0.1	<.001
	Reader 2	2.5 ± 0.2	3.2 ± 0.1	<.001
SNR	Reader 1	4.2 ± 0.1	3.7 ± 0.1	<.01
	Reader 2	2.7 ± 0.1	2.5 ± 0.1	<.05
Anatomic distortion	Reader 1	3.1 ± 0.2	4.3 ± 0.1	<.001
	Reader 2	3.0 ± 0.2	3.6 ± 0.1	<.01
Image sharpness	Reader 1	3.4 ± 0.1	3.5 ± 0.1	ns, .4
	Reader 2	3.4 ± 0.1	3.3 ± 0.1	ns, .4
Differentiation of pz and tz	Reader 1	4.1 ± 0.1	3.7 ± 0.1	<.001
	Reader 2	3.3 ± 0.1	3.4 ± 0.1	ns, 1.0
Overall image quality	Reader 1	3.5 ± 0.1	3.9 ± 0.1	<.05
	Reader 2	2.8 ± 0.2	3.1 ± 0.1	<.05
Diagnostic certainty	Reader 1	3.8 ± 0.1	4.1 ± 0.2	ns, .6
	Reader 2	3.4 ± 0.2	4.0 ± 0.1	<.01

Values are given as mean ± standard error of the mean. A 5-point Likert-scale was applied for the visual assessment of image quality: 1 = non-diagnostic, 2 = poor, 3 = satisfactory, 4 = good, 5 = excellent. *P*-values were derived from Wilcoxon rank sum tests.

ICC = intraclass correlation coefficient, Pz = peripheral zone, rsEPI = readout-segmented echoplanar imaging, SNR = signal-to-noise ratio, ssEPI = single-shot echoplanar imaging, tz = transition zone.

radical prostatectomy and active surveillance in low-grade and intermediate-grade PCa, focal therapies using MRI/ultrasound fusion-guided systems might gain rising importance.[32] In order to treat the complete tumorous tissue with focal therapy while preserving healthy adjacent tissue and surrounding structures, the correct localization and expansion of the target lesion is essential, underlining the importance of anatomical correct delineation on MRI.

Comparable to our results, higher prostate contour similarity with T2-weighted images has been reported with rsEPI than with ssEPI DWI in 10 healthy subjects in an objective assessment[33] and in phantom studies.[34] Also, a subjective assessment of clinical prostate MRI revealed a reduction of susceptibility artifacts and improved image quality in the pz with rsEPI DWI.[21] Similarly, reduced geometric distortion, image blurring, and artifact levels with rsEPI compared to ssEPI have been shown in subjective assessments of 47 breast MRI examinations[15] and in several head and neck studies.[18,19,35]

Contrary to the mentioned studies, a recent publication on different DWI techniques for prostate MRI in 10 healthy subjects did not show significant differences in image distortion between ssEPI and rsEPI.[20] A reason for the different results could be the different study populations: the mentioned study by Stocker et al included only young healthy subjects (mean age: 26 years old), not reflecting the typical population undergoing prostate MRI. The mean age in our study cohort was 69 years old and patients of that age are more likely to have hip replacements, vascular stents or other post-surgery conditions, as well as back-pain related motion artifacts. The importance of artifact-reduction with rsEPI compared to ssEPI becomes most evident in patients with metal implants (eg, hip prosthesis) or air-filled rectums, where the rsEPI sequence might be superior. Examples from our patient collective are given in Figure 2.

In our study, ADC values of the healthy prostatic tissue were significantly higher with rsEPI compared to ssEPI in the tz, but no significant difference was found for the target lesions and the healthy prostatic tissue of the pz. Xia et al found comparable results for rectal tumors with no significant difference in ADC values of tumorous lesions, and higher ADC in normal tissue with rsEPI.[36] But, so far, inhomogeneous results for the comparison of ADC measurements of the 2 DWI sequences have been published: no difference in ADC values has been reported in a recent study on phantom measurements[37] and in the prostate tissue of healthy subjects,[20] lower ADC values with rsEPI have been reported by Liney et al in their phantom measurements,[33] by Xu et al in orbital tumors[35] and by Zhao et al in sinonasal lesions.[17] Still, ADC values have been inconsistent across vendors and are influenced by multiple parameters, for example, by the choice of *b*-values (reflecting perfusion and diffusion properties in different fractions).[5] Therefore no clear conclusion can be drawn from these reported ADC measurements without distinct standardization of imaging parameters. Nevertheless, values of calculated ssEPI ADC maps with 2 or 3 *b*-values did not result in significant different ADC-values in our study.

In our study, image contrast was higher on b1000 images of rsEPI compared to ssEPI. Similarly, higher image contrast was reported on ADC maps of rsEPI DWI compared to ssEPI DWI on breast MRI[15] and MRI studies on orbital tumors,[35] potentially enabling better visual discrimination of benign and malignant tissue.

We found that CNR was not significantly different in the comparison of ssEPI and rsEPI, neither on ADC maps nor on b1000 images. However, subjective SNR was rated higher on ssEPI compared to rsEPI in the visual assessment in our study. Controversial results on CNR and SNR have been published before: higher CNR and SNR for rsEPI compared to ssEPI has been reported for MRI studies on rectal cancer[36] and on renal MRI in animal studies[38]; lower SNR has been found by Xu et al[35] in orbital tumors, by Bogner et al[15] in breast examinations and by Zhao et al[17] in sinonasal lesions; no significant CNR difference has also been reported in several studies.[15,17,35] In order to acquire conclusive data on SNR and CNR, standardized protocols should be defined and applied in further and larger study cohorts, since SNR can be influenced by several factors and MR parameters.

Nevertheless, we showed good diagnostic ability for the detection of PCa with ADC values of both DWI sequences (Fig. 3). Youden-selected cut-off values of ADC for the detection of PCa were $0.971*10^{-3}$ mm^2/s for rsEPI and $1.017*10^{-3}$ mm^2/s

for ssEPI. The PI-RADS version 2 document suggests a threshold of 0.75–0.9*10^{-3} mm^2/s, that may assist differentiation between benign and malignant prostate tissues in the pz, and that lower ADC values correlate with clinically significant cancer.[5] Still, the Youden-selected cut-off value only reflects a calculated value that could not be used in a clinical setting due to the risk of a high number of false-negative results. The choice of the cut-off value with the Youden-index assumes that sensitivity and specificity are equally important and maximizes the statistic value of diagnostic accuracy but not necessarily meets the criteria for imaging reporting in a clinical setting.

Our study has limitations. First, we did not quantify SNR in our study due to the MRI protocol that was used according to recommendations of the ACR, AdMeTech Foundation, and ESUR. The easiest method for SNR measurements would have been to quantify signal intensity and standard deviation of the adjacencies outside of the patients' body, but our field of view focused on the organ of interest and did not include the surrounding adjacencies. The difference method[39,40] could have been an alternative, but we decided that a second acquisition of both DWI sequences would inadequately prolong examination time, resulting in incompliance of patients. Second, our population included patients with high-grade and intermediate-grade PCa according to standard definitions (n=12 with Gleason 3+3=6, n=23 with Gleason ≥3+4=7) and no distinction was made in our analysis due to low patient numbers in the subgroups. However, the definition of a clinically significant PCa is not standardized. Furthermore, only patients with MRI visible suspicious lesions underwent biopsy; therefore a false-negative rate could not be determined.

In conclusion, we could demonstrate comparable high diagnostic ability for the detection of PCa with ADC values of ssEPI DWI and rsEPI DWI. Quantified CNR was comparable and image contrast was higher with rsEPI and ssEPI on b1000-images while SNR was higher with ssEPI in the visual assessment. Anatomic delineation was significantly better and image quality higher with rsEPI than with ssEPI and it might, therefore, be more suitable for prostate MRI, particularly with regard to targeted MRI-guided biopsy and focal therapy.

Author contributions

Conceptualization: Susanne Hellms, Marcel Gutberlet, Inga Peters, Wacker Frank, Katja Derlin.
Data curation: Susanne Hellms, Matti Joonas Peperhove, Stefanie Pertschy, Christoph Henkenberens, Wacker Frank, Katja Derlin.
Formal analysis: Susanne Hellms, Marcel Gutberlet, Matti Joonas Peperhove, Katja Derlin.
Funding acquisition: Susanne Hellms, Katja Derlin.
Investigation: Susanne Hellms, Matti Joonas Peperhove, Inga Peters, Katja Derlin.
Methodology: Susanne Hellms, Marcel Gutberlet, Matti Joonas Peperhove, Stefanie Pertschy, Christoph Henkenberens, Inga Peters, Wacker Frank, Katja Derlin.
Project administration: Susanne Hellms, Inga Peters, Wacker Frank, Katja Derlin.
Resources: Susanne Hellms, Stefanie Pertschy, Wacker Frank, Katja Derlin.
Software: Marcel Gutberlet, Wacker Frank, Katja Derlin.
Supervision: Susanne Hellms, Marcel Gutberlet, Wacker Frank, Katja Derlin.
Validation: Susanne Hellms, Matti Joonas Peperhove, Inga Peters, Katja Derlin.
Visualization: Katja Derlin.
Writing – original draft: Susanne Hellms, Marcel Gutberlet, Katja Derlin.
Writing – review and editing: Susanne Hellms, Marcel Gutberlet, Matti Joonas Peperhove, Stefanie Pertschy, Christoph Henkenberens, Inga Peters, Wacker Frank, Katja Derlin.

Susanne Hellms orcid: 0000-0001-9604-2691.

References

[1] Boesen L. Multiparametric MRI in detection and staging of prostate cancer. Dan Med J 2017;64:B5327pages 1–25.
[2] de Rooij M, Hamoen EH, Futterer JJ, et al. Accuracy of multiparametric MRI for prostate cancer detection: a meta-analysis. AJR Am J Roentgenol 2014;202:343–51.
[3] Valerio M, Donaldson I, Emberton M, et al. Detection of clinically significant prostate cancer using magnetic resonance imaging-ultrasound fusion targeted biopsy: a systematic review. Eur Urol 2015;68:8–19.
[4] Dickinson L, Ahmed HU, Allen C, et al. Magnetic resonance imaging for the detection, localisation, and characterisation of prostate cancer: recommendations from a European consensus meeting. Eur Urol 2011;59:477–94.
[5] Weinreb JC, Barentsz JO, Choyke PL, et al. PI-RADS prostate imaging - reporting and data system: 2015, version 2. Eur Urol 2016;69:16–40.
[6] Bratan F, Niaf E, Melodelima C, et al. Influence of imaging and histological factors on prostate cancer detection and localisation on multiparametric MRI: a prospective study. Eur Radiol 2013;23:2019–29.
[7] Schimmoller L, Quentin M, Arsov C, et al. MR-sequences for prostate cancer diagnostics: validation based on the PI-RADS scoring system and targeted MR-guided in-bore biopsy. Eur Radiol 2014;24:2582–9.
[8] Nagel KN, Schouten MG, Hambrock T, et al. Differentiation of prostatitis and prostate cancer by using diffusion-weighted MR imaging and MR-guided biopsy at 3 T. Radiology 2013;267:164–72.
[9] Osugi K, Tanimoto A, Nakashima J, et al. What is the most effective tool for detecting prostate cancer using a standard MR scanner? Magn Reson Med Sci 2013;12:271–80.
[10] Isebaert S, Van den Bergh L, Haustermans K, et al. Multiparametric MRI for prostate cancer localization in correlation to whole-mount histopathology. J Magn Reson Imaging 2013;37:1392–401.
[11] Gibbs P, Liney GP, Pickles MD, et al. Correlation of ADC and T2 measurements with cell density in prostate cancer at 3.0 Tesla. Invest Radiol 2009;44:572–6.
[12] Schoots IG, Roobol MJ, Nieboer D, et al. Magnetic resonance imaging-targeted biopsy may enhance the diagnostic accuracy of significant prostate cancer detection compared to standard transrectal ultrasound-guided biopsy: a systematic review and meta-analysis. Eur Urol 2015;68:438–50.
[13] Siddiqui MM, Rais-Bahrami S, Turkbey B, et al. Comparison of MR/ultrasound fusion-guided biopsy with ultrasound-guided biopsy for the diagnosis of prostate cancer. JAMA 2015;313:390–7.
[14] Porter DA, Heidemann RM. High resolution diffusion-weighted imaging using readout-segmented echo-planar imaging, parallel imaging and a two-dimensional navigator-based reacquisition. Magn Reson Med 2009;62:468–75.
[15] Bogner W, Pinker-Domenig K, Bickel H, et al. Readout-segmented echo-planar imaging improves the diagnostic performance of diffusion-weighted MR breast examinations at 3.0 T. Radiology 2012;263:64–76.
[16] Xu XQ, Liu J, Hu H, et al. Improve the image quality of orbital 3 T diffusion-weighted magnetic resonance imaging with readout-segmented echo-planar imaging. Clin Imaging 2016;40:793–6.
[17] Zhao M, Liu Z, Sha Y, et al. Readout-segmented echo-planar imaging in the evaluation of sinonasal lesions: a comprehensive comparison of image quality in single-shot echo-planar imaging. Magn Reson Imaging 2016;34:166–72.
[18] Algin O, Aydin H, Ozmen E, et al. Detection of cholesteatoma: high-resolution DWI using RS-EPI and parallel imaging at 3 tesla. J Neuroradiol 2017;44:388–94.
[19] Morelli J, Porter D, Ai F, et al. Clinical evaluation of single-shot and readout-segmented diffusion-weighted imaging in stroke patients at 3 T. Acta Radiol 2013;54:299–306.

[20] Stocker D, Manoliu A, Becker AS, et al. Image quality and geometric distortion of modern diffusion-weighted imaging sequences in magnetic resonance imaging of the prostate. Invest Radiol 2018;53:200–6.
[21] Li L, Wang L, Deng M, et al. Feasibility study of 3-T DWI of the prostate: readout-segmented versus single-shot echo-planar imaging. AJR Am J Roentgenol 2015;205:70–6.
[22] Shoji S, Hiraiwa S, Endo J, et al. Manually controlled targeted prostate biopsy with real-time fusion imaging of multiparametric magnetic resonance imaging and transrectal ultrasound: an early experience. Int J Urol 2015;22:173–8.
[23] Tewes S, Hueper K, Hartung D, et al. Targeted MRI/TRUS fusion-guided biopsy in men with previous prostate biopsies using a novel registration software and multiparametric MRI PI-RADS scores: first results. World J Urol 2015;33:1707–14.
[24] Tewes S, Peters I, Tiemeyer A, et al. Evaluation of MRI/ultrasound fusion-guided prostate biopsy using transrectal and transperineal approaches. Biomed Res Int 2017;2017:2176471.
[25] Stejskal E. Use of spin echoes in a pulsed magnetic-field gradient to study anisotropic restricted diffusion and flow. J Chem Phys 1965;43:3597–603.
[26] Bogner W, Gruber S, Pinker K, et al. Diffusion-weighted MR for differentiation of breast lesions at 3.0 T: how does selection of diffusion protocols affect diagnosis? Radiology 2009;253:341–51.
[27] DeLong ER, DeLong DM, Clarke-Pearson DL. Comparing the areas under two or more correlated receiver operating characteristic curves: a nonparametric approach. Biometrics 1988;44:837–45.
[28] Tewes S, Mokov N, Hartung D, et al. Standardized reporting of prostate MRI: comparison of the prostate imaging reporting and data system (PI-RADS) version 1 and version 2. PLoS One 2016;11:e0162879.
[29] Delongchamps NB, Rouanne M, Flam T, et al. Multiparametric magnetic resonance imaging for the detection and localization of prostate cancer: combination of T2-weighted, dynamic contrast-enhanced and diffusion-weighted imaging. BJU Int 2011;107:1411–8.
[30] Moore CM, Robertson NL, Arsanious N, et al. Image-guided prostate biopsy using magnetic resonance imaging-derived targets: a systematic review. Eur Urol 2013;63:125–40.
[31] Radtke JP, Kuru TH, Boxler S, et al. Comparative analysis of transperineal template saturation prostate biopsy versus magnetic resonance imaging targeted biopsy with magnetic resonance imaging-ultrasound fusion guidance. J Urol 2015;193:87–94.
[32] Franz T, von Hardenberg J, Blana A, et al. MRI/TRUS fusion-guided prostate biopsy: value in the context of focal therapy. Urologe A 2017;56:208–16.
[33] Liney GP, Holloway L, Al Harthi TM, et al. Quantitative evaluation of diffusion-weighted imaging techniques for the purposes of radiotherapy planning in the prostate. Br J Radiol 2015;88:20150034.
[34] Foltz WD, Porter DA, Simeonov A, et al. Readout-segmented echo-planar diffusion-weighted imaging improves geometric performance for image-guided radiation therapy of pelvic tumors. Radiother Oncol 2015;117:525–31.
[35] Xu X, Wang Y, Hu H, et al. Readout-segmented echo-planar diffusion-weighted imaging in the assessment of orbital tumors: comparison with conventional single-shot echo-planar imaging in image quality and diagnostic performance. Acta Radiol 2017;58:1457–67.
[36] Xia CC, Liu X, Peng WL, et al. Readout-segmented echo-planar imaging improves the image quality of diffusion-weighted MR imaging in rectal cancer: comparison with single-shot echo-planar diffusion-weighted sequences. Eur J Radiol 2016;85:1818–23.
[37] Walter SS, Liu W, Stemmer A, et al. Combination of integrated dynamic shimming and readout-segmented echo planar imaging for diffusion weighted MRI of the head and neck region at 3Tesla. Magn Reson Imaging 2017;42:32–6.
[38] Wu CJ, Wang Q, Zhang J, et al. Readout-segmented echo-planar imaging in diffusion-weighted imaging of the kidney: comparison with single-shot echo-planar imaging in image quality. Abdom Radiol (NY) 2016;41:100–8.
[39] Dietrich O, Raya JG, Reeder SB, et al. Measurement of signal-to-noise ratios in MR images: influence of multichannel coils, parallel imaging, and reconstruction filters. J Magn Reson Imaging 2007;26:375–85.
[40] Goerner FL, Clarke GD. Measuring signal-to-noise ratio in partially parallel imaging MRI. Med Phys 2011;38:5049–57.